Check for updates

Han-Ling Li
Key Laboratory of Thermal Science and Power Engineering of Education of Ministry, Department of Mechanical Engineering, Tsinghua University, Beijing 10084, China
e-mail: lihanling1994@163.com

Yang Shen
Key Laboratory of Thermal Science and Power Engineering of Education of Ministry, Department of Mechanical Engineering, Tsinghua University, Beijing 10084, China
e-mail: sheny21@mails.tsinghua.edu.cn

Yu-Chao Hua
LTEN Laboratory Polytech Nantes, University of Nantes, Nantes, UMR6607, F-44000, France
e-mail: huayuchao19@163.com

S. L. Sobolev
Department of Theoretical Physics, Institute of Problems of Chemical Physics, Academy of Sciences of Russia, Chernogolovka, Moscow Region 142432, Russia
e-mail: sobolev@icp.ac.ru

Bing-Yang Cao[1]
Key Laboratory of Thermal Science and Power Engineering of Education of Ministry, Department of Mechanical Engineering, Tsinghua University, Beijing 10084, China
e-mail: caoby@mail.tsinghua.edu.cn

Hybrid Monte Carlo-Diffusion Studies of Modeling Self-Heating in Ballistic-Diffusive Regime for Gallium Nitride HEMTs

Exact assessment of self-heating is of great importance to the thermal management of electronic devices, especially when completely considering the cross-scale heat conduction process. The existing simulation methods are either based on convectional Fourier's law or limited to small system sizes, making it difficult to deal with noncontinuum thermal transport efficiently. In this paper, a hybrid phonon Monte Carlo diffusion method is adopted to predict device temperature in ballistic–diffusive regime. Heat conduction around the heat generation region and boundaries are simulated by phonon Monte Carlo (MC) method, while the other domain is by Fourier's law. The temperature of the hybrid method is higher than that of Fourier's law owing to phonon ballistic transport, and the calculation efficiency of the hybrid method is remarkably improved compared with phonon MC simulation. Furthermore, the simulation results indicate that the way of modeling self-heating has a remarkable impact on phonon transport. The junction temperature of the heat source (HS) scheme can be larger than that of the heat flux (HF) scheme, which is opposite to the result under Fourier's law. In the HS scheme, the enhanced phonon-boundary scattering counteracts the broadening of the heat source, leading to a stronger ballistic effect and higher temperatures. The conclusion is verified by a one-dimensional analytical model. This work has opened up an opportunity for the fast and extensive thermal simulations of cross-scale heat transfer in electronic devices and highlighted the influence of heating schemes. [DOI: 10.1115/1.4054698]

Keywords: self-heating, ballistic-diffusive heat conduction, hybrid Monte Carlo-diffusion method, high-electron-mobility transistor (HEMT)

1 Introduction

Owing to its advantages in high breakdown voltage and large bandgap, the gallium nitride (GaN) high-electron-mobility transistor (HEMT) is an excellent choice for high-voltage and high-frequency power electronic devices [1,2]. The power improvement in GaN HEMTs inevitably leads to huge power density ($>10\,\mathrm{kW/cm^2}$) [3] and elevated junction temperature, this self-heating results in significant thermal bottlenecks of these devices [4–8]. The typical structure of GaN HEMTs is shown in Fig. 1, and its basic form is made of multilayer films. During operation, heat is primarily generated in the channel layer under the drain side edge of the gate [9], the width of the heat generation region is of the order of 100 nm, while the thickness is of the order of 1 nm [10–12]. The thickness of the channel layer is usually 1–3 μm, whereas the thickness of the substrate is larger than 100 μm. It is worth noting that the length and width of the channel layer can reach the order of 1 mm. In this way, the generated heat will spread from a small area to a much larger substrate, as the arrows in Fig. 1 show. This phenomenon produces a multidimensional temperature field and a conspicuous near junction resistance, which is also known as thermal spreading resistance [13]. In addition, the thicknesses of the heat generation region, channel layer, and substrate vary several orders of magnitude, resulting in a cross-scale heat conduction process. Since it is a pivotal problem in the heat transfer of HEMTs, accurate and efficient evaluation of self-heating is critical to estimate the performance and assess the reliability, as well as developing innovative thermal designs [14–17].

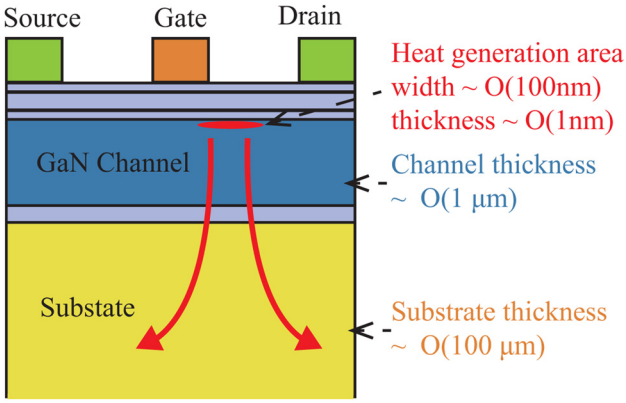

Fig. 1 Schematic of GaN HEMTs

[1]Corresponding author.

Contributed by the Electronic and Photonic Packaging Division of ASME for publication in the Journal of Electronic Packaging. Manuscript received February 21, 2022; final manuscript received May 25, 2022; published online July 13, 2022. Assoc. Editor: Ronald Warzoha.

 Copyright © 2023 by ASME

Downloaded from http://asmedigitalcollection.asme.org/electronicpackaging/article-pdf/145/1/011203/6976220/ep_145_01_011203.pdf by Tsinghua University user on 01 February 2023

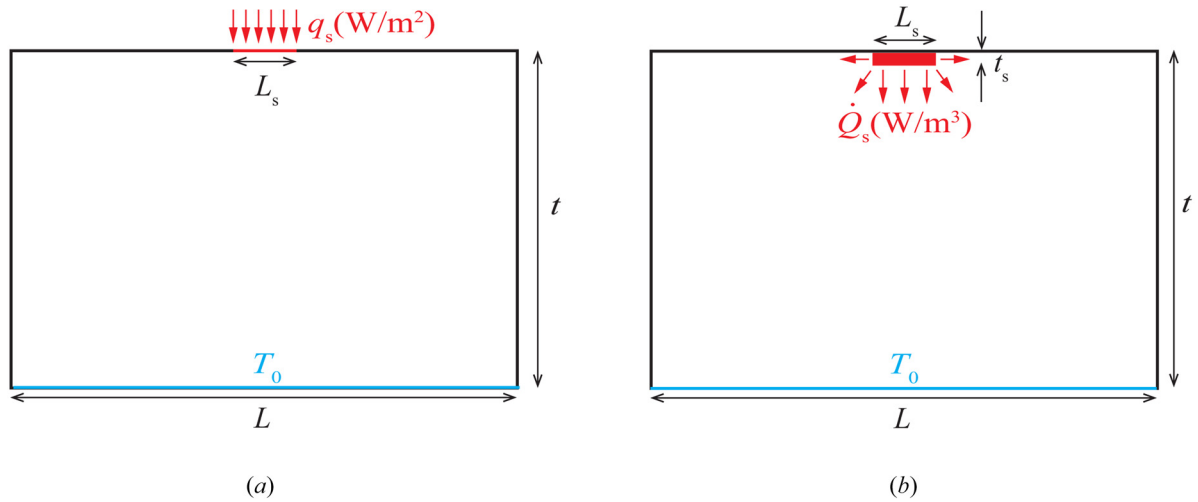

Fig. 2 Two schemes of modeling self-heating: (*a*) the surface heat flux (HF) scheme and (*b*) the volumetric heat source (HS) scheme

Based on Fourier's heat conduction law [18], a large amount of work has been reported on the analyses of self-heating. Krane [19] established analytical models for the temperature and thermal resistance under the conditions of a concentric heat source on rectangle channels. Then, Muzychka et al. [20] studied the cases of eccentric and discrete heat sources, and Darwish et al. [21] investigated the effect of the substrate. Moreover, the model has been expanded to consider the interfacial thermal resistance [22], the anisotropy of thermal conductivity [23], the arbitrary number of layers [24], and the temperature-dependent thermal conductivity [25]. Recently, Pearson et al. [26] explored the accuracy of common assumptions made in GaN HEMT channel temperature thermal analyses with an electrohydrodynamic model coupled with Fourier's law and provided modeling guidelines. In these papers, self-heating is typically modeled as the surface heat flux on the top boundary of the system, which we call the heat flux (HF) heating scheme, as Fig. 2(*a*) shows. However, directly adopting Fourier's law to heat transfer in micro- and nano-scale electronic devices will cause some errors [27–29]. Mean-free-paths (MFPs) of phonons (the major heat carriers in semiconductors) for GaN are approximately 100 nm to 10 μm [30–32], which are comparable to the width of heat generation region and thickness of the channel layer in GaN HEMTs. As a result, phonon ballistic transport emerges [33,34], and ballistic–diffusive heat conduction raises the junction temperature to be higher than the prediction of Fourier's law [35–38].

Efforts have been devoted to exploring the characteristics of ballistic–diffusive heat conduction and accounting for phonon ballistic transport in the thermal analyses of electronic devices. Cao and Li [39,40] studied the effective thermal conductivity of nanostructures by nonequilibrium molecular dynamics simulations and found that the results of the uniform heat source scheme are much lower than those of the temperature difference scheme. Using phonon Monte Carlo (MC) simulations, Hua and Cao [41] obtained similar results and established a theoretical model for the effective thermal conductivity in the internal heat source scheme. Then, it is claimed that the models of the effective thermal conductivities can be unified as a function of the Knudsen number (ratio of phonon MFP to the characteristic length) and the shape factor [42]. Recently, Hua et al. [43] investigated the heat dissipation of GaN HEMTs in ballistic-diffusive regime under the HF heating scheme and demonstrated that there are two ballistic effects affecting heat transfer: one is related to the cross-plane Knudsen number and the other is related to the lateral Knudsen number. These studies suggest that the geometric size and heating scheme play a significant role in ballistic-diffusive heat conduction. However, subject to computational complexity and costs, molecular dynamics or phonon MC is limited to small systems and cannot simulate the cross-scale heat transfer process in real electronic devices [44]. The hybrid method that combines the accuracy of the micro- and nano-scale simulation techniques and the simplicity of Fourier's law is a promising way to overcome this problem [45]. By solving phonon Boltzmann transport equation (BTE) in a small domain of the device channel and utilizing Fourier's law in the rest domain, Donmezer and Graham [10] found that the hotspot temperature is higher when the ballistic-diffusive transport effect is considered. Hao et al. [46] combined phonon MC and Fourier's law in a similar way to simulate two-dimensional (2D) GaN HEMTs, then the method was applied to more complex structures [47,48]. Chatterjee et al. [12] proposed a phonon BTE—Fourier coupled thermal modeling to study the interplay of heat concentration and ballistic effect. These reports successfully simulate the heat transfer of GaN HEMTs in particular sizes, but detailed research of the junction temperature in systems with a relatively large size is still lacking. Moreover, these works not only used a hybrid multiscale thermal simulation technique, but also employed electrical simulations to predict the heat generation distribution. They reported a volumetric heat generation region with nonzero thickness, as shown in Fig. 2(*b*), which we call the heat source (HS) heating scheme. The HS heating scheme agrees better with electrical simulations than the HF scheme and is expected to be more suitable for modeling self-heating, but the difference between the HF scheme and HS scheme in the calculation of temperature remains unclear, especially considering the fact that the heating scheme does affect phonon transport in ballistic–diffusive heat conduction of nanofilms.

In this paper, a hybrid phonon MC-diffusion method is employed to study the self-heating in ballistic–diffusive regime. By dividing the whole system and coupling phonon MC simulation with Fourier's law, the hybrid method is capable of characterizing the heat transfer process as accurately as phonon MC simulation while greatly scaling down the computational time, facilitating the fast simulation of ballistic–diffusive heat conduction over a comprehensive size range. The validity of the hybrid method is verified by comparison with experimental measurements. Furthermore, the way of modeling self-heating is found to have a remarkable impact on phonon transport, and the ballistic effect in the HS scheme can be much stronger than that in the HF scheme as the thickness of the heat generation region declines. Parametric investigations and theoretical analyses claim that this can be interpreted by the variation in the heat source spatial distribution and phonon-boundary scattering. It is recommended to utilize the HS scheme to model self-heating in GaN HEMTs.

Downloaded from http://asmedigitalcollection.asme.org/electronicpackaging/article-pdf/145/1/011203/6976220/ep_145_01_011203.pdf by Tsinghua University user on 01 February 2023

2 Methods

The research objects of this work are shown in Fig. 2, which are representative 2D simplified models for the heat dissipation processes in GaN HEMTs. For the HF scheme shown in Fig. 2(*a*), self-heating is modeled as a boundary heat flux condition with the heat flux being q_s and the length being L_s. As a contrast, the HS scheme shown in Fig. 2(*b*) models self-heating as a volumetric heat source in a rectangle region of size $L_s \times t_s$ with a power dissipation density of $\dot{Q}_s$. The difference between the two heating schemes will be investigated by numerical simulations as well as theoretical analyses. Other boundary conditions are consistent with [43], namely, fixed temperature T_0 at the bottom boundary, adiabatic at the top boundary, and periodic at the lateral boundaries.

The hybrid MC-diffusion method developed in Ref. [49] is employed to characterize ballistic–diffusive heat conduction, as shown in Fig. 3 where the HS scheme is taken as an example. Based on the idea that ballistic transport mainly affects the regions adjacent to the phonon source and boundaries when the system is considerably large, the whole computational domain is divided into three zones: the top MC zone that covers the heat generation region and top boundary, the bottom MC zone that covers the bottom boundary, and the middle diffusion zone. There are overlap zones between the MC and diffusion zones to transfer information and check convergence. The thicknesses of the top MC zone, bottom MC zone, and overlap zone are denoted as t_{topMC}, t_{botMC}, and t_o. Compared with the hybrid BTE-Fourier methods in Refs. [12] and [46–48], there is an additional bottom MC zone, of which the necessity will be explained in Sec. 3.1.

Phonon MC simulation and the finite element method (FEM) based on Fourier's law are coupled by an alternating technique in the hybrid method. The flowchart of the hybrid method is illustrated in Fig. 4, which has the following procedures: *(i) Initialization:* Use the FEM to obtain the diffusive solution of the problem. *(ii) Phonon MC simulation:* Use the heat flux obtained by FEM as boundary conditions at the interfaces from the MC zones to the diffusion zone and run phonon MC simulation. *(iii) Middle diffusion solution:* Alternate the boundary temperature and heat flux at the interfaces from the diffusion zone to the MC zones by the results of MC simulations and run FEM. *(iv) Hotspot temperature refinement:* Run the MC simulation again in the top MC domain with the FEM-updated boundary temperature. *(v) Convergence judgment:* If the temperature and heat flux distribution of phonon MC and FEM converge to equality in the overlap zones, the calculation ends; otherwise it proceeds to (ii) and repeats.

In this paper, the gray-body approximation that assumes all phonons have the same MFP (denoted as Λ) is used to simplify the problem. With a proper and representative choice of the MFP, the results of the gray-body approximation are in good agreement with the results on account of phonon dispersion as well as experimental measurements [50]. In-depth discussions about the effect of phonon dispersion on the temperature of devices have been carried out elsewhere [51]. Noting that the size of the region affected

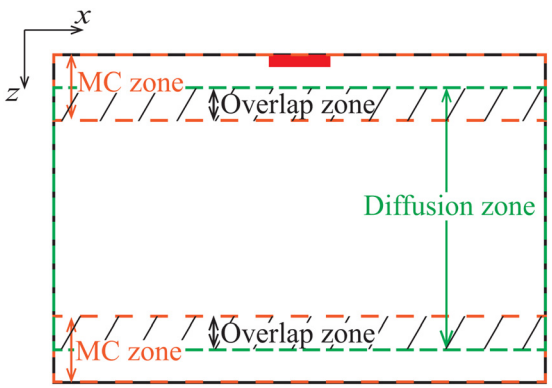

Fig. 3 Schematic of the domain dividing

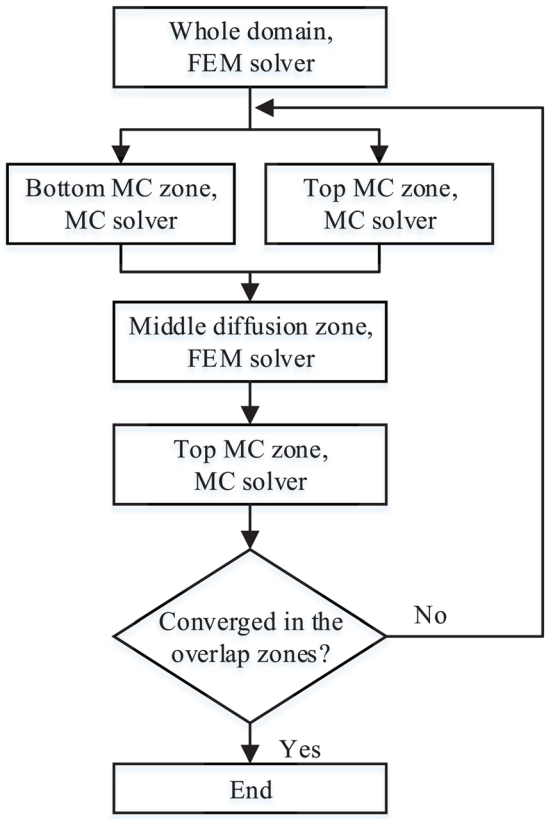

Fig. 4 Flowchart of the hybrid MC-diffusion method

by the phonon source or phonon absorbing boundary is around one phonon MFP [35], the sizes of the MC zones and overlap zones are set as $t_{topMC} = \max(2.0\Lambda, t_s + 1.5\Lambda)$, $t_{botMC} = 2.0\Lambda$, $t_o = 1.0\Lambda$ [49]. Such settings obtain a pleasant balance between the calculation accuracy and efficiency. The number of simulated phonon bundles is 10^7, which is large enough to suppress the random error originating from the statistical nature of MC simulation. Details of phonon MC simulation and the hybrid MC-diffusion method can be found in Refs. [37] and [49], respectively.

Based on Fourier's law, it is suggested that accurate temperature prediction of GaN HEMTs requires modeling heat generation by electrical simulations, establishing a three-dimensional numerical model, choosing representative thermal properties for each composite layer of the device, considering thermal boundary resistance (TBR), and employing physically reasonable Robin boundary conditions [26]. Considering these factors does not qualitatively affect the influence of phonon ballistic transport and its dependence on size parameters, but significantly increases the complexity and solving cost of the problem. Since the aim of this paper is to consider phonon ballistic transport in the prediction of temperatures by a multiscale hybrid method and distinguish the surface HF heating scheme from the volumetric HS heating scheme, to simply the analyses and focus on what we are concerned with, some assumptions are made, including using constant heating power as at $P = L_s q_s = L_s t_s \dot{Q}_s = 0.2\,\mathrm{W/m}$ without electrical simulations, modeling 2D systems, using material properties at 300 K, adopting Dirichlet boundary condition with $T_0 = 300\,\mathrm{K}$. It should be noted that the accuracy of the hybrid MC-diffusion method in this paper is relative to phonon MC simulation and is not influenced by these assumptions.

3 Results and Discussions

3.1 Validation of the Hybrid Monte Carlo-Diffusion Method. At first, the performance of the hybrid MC-diffusion method in modeling self-heating is examined. As further

Downloaded from http://asmedigitalcollection.asme.org/electronicpackaging/article-pdf/145/1/011203/6976220/ep_145_01_011203.pdf by Tsinghua University user on 01 February 2023

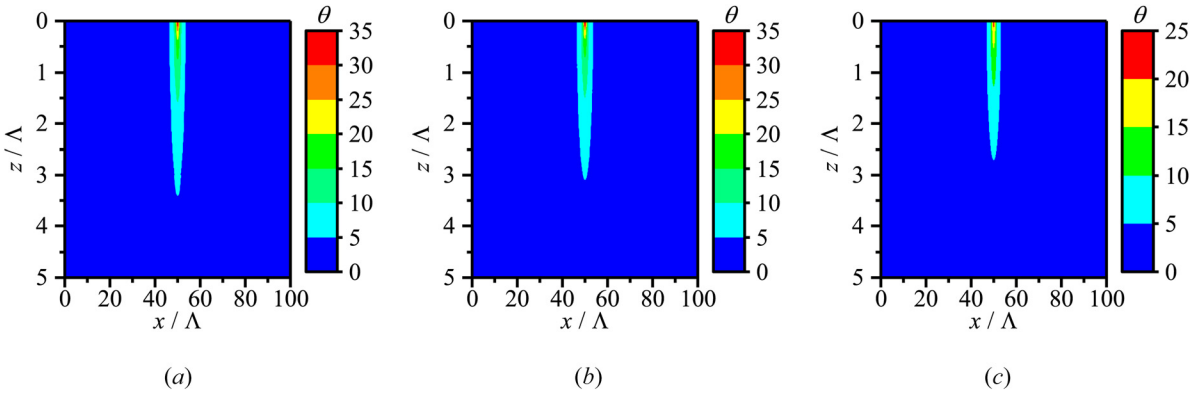

Fig. 5 Dimensionless temperature distributions calculated by: (*a*) hybrid MC-diffusion method, (*b*) MC simulation, and (*c*) FEM. The sizes are $Kn_L = 0.01$, $Kn_t = 0.2$, $Kn_{L,s} = 1$, $Kn_{t,s} = 10$.

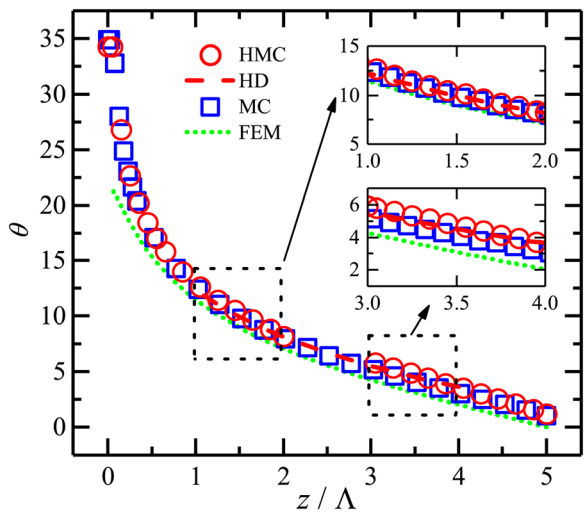

Fig. 6 Dimensionless temperature at the vertical symmetry line ($Kn_L = 0.01$, $Kn_t = 0.2$, $Kn_{L,s} = 1$, $Kn_{t,s} = 10$). "HMC" and "hybrid diffusion" denote the hybrid MC and hybrid diffusion, respectively. The insets show the enlarged figures of the top and bottom overlap zones with more nodes displayed.

simplifications, the substrate material is assumed to be the same as the channel material, and their interfacial TBR is also ignored. In this way, phonon MC simulation can be implemented with moderate computational costs and used as a benchmark. Self-heating is modeled as the volumetric HS heating, as shown in Fig. 2(*b*). According to the typical size of GaN HEMT, the four geometry parameters in the test case are set as $Kn_L = 0.01$, $Kn_t = 0.2$, $Kn_{L,s} = 1$, $Kn_{t,s} = 10$, in which Kn denotes the Knudsen number. The dimensionless temperature distributions predicted by the hybrid MC-diffusion method are shown in Fig. 5(*a*). As a comparison, the results calculated by the MC simulation and FEM are depicted in Figs. 5(*b*) and 5(*c*), respectively. The dimensionless temperature is defined as $\theta = (T - T_0)/(\dot{Q}_s L_s t_s R_{1D,0})$ where $R_{1D,0} = t/(Lk_{bulk})$ is the one-dimensional (1D) diffusive thermal resistance in the HF scheme [43]. The temperature distribution of the hybrid MC-diffusion method is in reasonable agreement with that of the MC simulation; they both predict longer and narrower hot areas and higher peak temperatures than the FEM results, indicating that the hybrid MC-diffusion method successfully characterizes phonon ballistic transport.

To better reveal the accuracy of the hybrid MC-diffusion method, the dimensionless temperature along the z direction at the vertical symmetry line is drawn in Fig. 6. The temperature convergence of the hybrid MC (HMC) and hybrid diffusion at the two overlap zones is clearly demonstrated by the insets, the result of the hybrid MC-diffusion method is $\theta_{max,hybrid} = 34.2$, while the value of the MC simulation is $\theta_{max,MC} = 34.9$, and their relative error is only about 2%. Compared to the FEM results, the temperature profile of the hybrid MC-diffusion method is always higher, even in the bottom MC zone ($3\Lambda \le z \le 5\Lambda$). Although the bottom MC zone has a distance of more than 3Λ from the heat generation region, since the system thickness is only a few phonon MFPs, phonon-boundary scattering at the bottom boundary has played a remarkable role, leading to a slight but obvious boundary temperature jump [52]. Therefore, Fourier's law fails at the regions near the bottom boundary, and it is necessary to introduce the bottom MC zone in the hybrid method to capture such a boundary nonequilibrium phenomenon.

In addition, the temperature distribution at the top of the system, which could be experimentally measured in a real HEMT [12], is drawn in Fig. 7. As expected, the hybrid MC-diffusion method agrees well with the MC simulation and predicts a considerably higher temperature than FEM around the heat generation region. Away from the heat generation region, the difference between hybrid the MC-diffusion method and FEM fades out, and the temperature can be calculated by Fourier's law. It is worth noting that most phonon movement and scattering occur near the heat generation region, to which the vast majority of computing resources are devoted under the energy-based variance-reduced MC framework [53]. The area other than the heat generation region contributes little to the computational cost, so the current

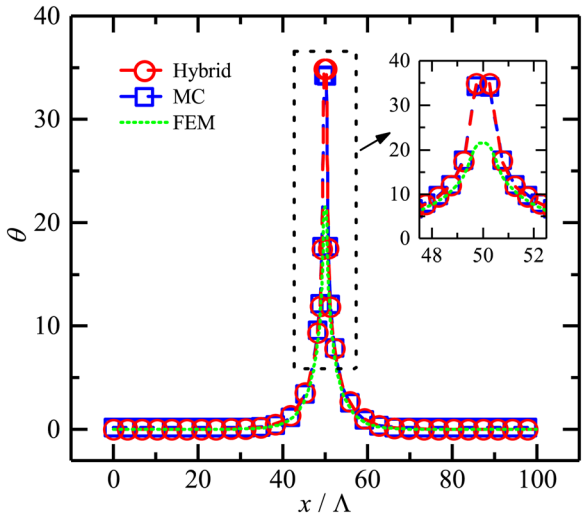

Fig. 7 Dimensionless temperature at the top boundary ($Kn_L = 0.01$, $Kn_t = 0.2$, $Kn_{L,s} = 1$, $Kn_{t,s} = 10$)

Downloaded from http://asmedigitalcollection.asme.org/electronicpackaging/article-pdf/145/1/011203/6976220/ep_145_01_011203.pdf by Tsinghua University user on 01 February 2023

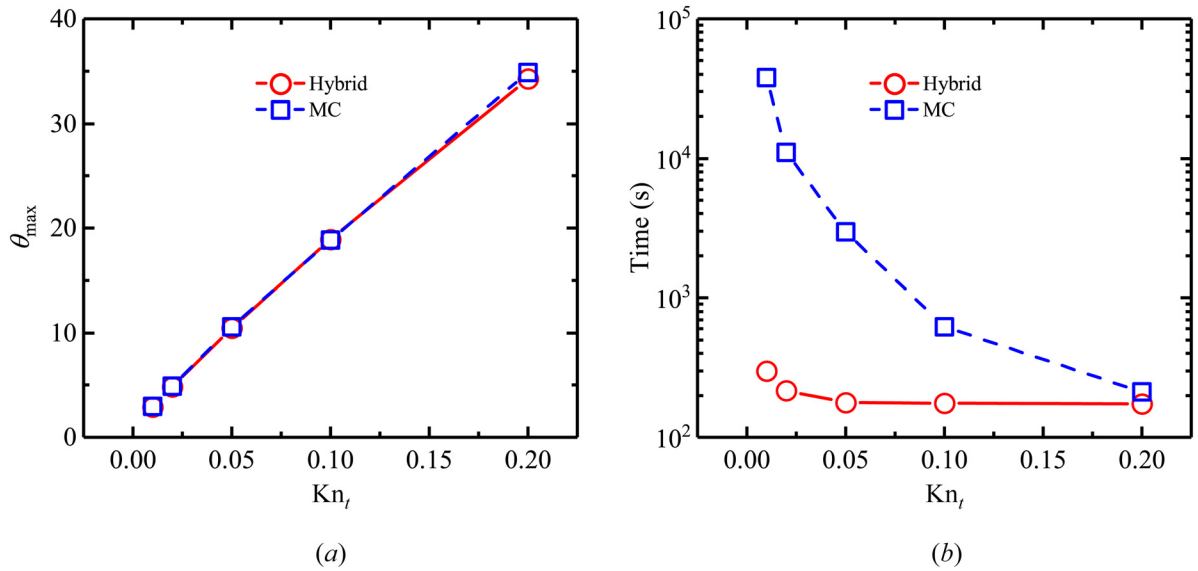

Fig. 8 (*a*) Dimensionless junction temperature varying with Kn_t and (*b*) computational time varying with Kn_t

hybrid method lets the length of the top MC zone be the same as the system length to simplify the iteration process.

More geometric structures are calculated to test the accuracy and efficiency of the hybrid MC-diffusion method. Figure 8 illustrates the dimensionless junction temperature and computational time of the hybrid MC-diffusion method varying with the system thickness, while the other three geometry parameters are kept the same. As a benchmark, the results of the MC simulation are also given. It can be seen that the hybrid method has a much better efficiency compared to the MC simulation without causing significant deviation on θ_{max}, and the computational time can be mostly reduced by up to 2 orders of magnitude, from tens of thousands seconds to hundreds of seconds. MC simulation could be an efficient tool when Kn_t is relatively large, as its computation time greatly decreases with Kn_t. For the hybrid MC-diffusion method, since the main time-consuming process is the MC simulation in the MC zones, the computation time is expected to be a constant as the sizes of the MC zone are fixed, which is verified by the nearly horizontal solid line in Fig. 8(*b*). The small oscillations are due to the different number of iterations required for convergence. It is recommended that for $Kn_t > 0.2$, there is no need to use the hybrid MC-diffusion method because the MC simulation is fast enough.

Then, the hybrid MC-diffusion method is used to simulate the heat dissipation in a GaN-on-SiC device sample to test its performance for more practical problems. The cross section of the sample is similar to Fig. 1; it consists of a substrate layer of SiC, a nucleation layer of AlN, a channel layer of GaN, and an insulation layer of SiO_2, of which the thicknesses are 350 μm, 50 nm, 2.1 μm, and 50 nm, respectively. The length and width of the sample are 7.5 mm. On the top of the insulation layer is an Au electrode that acts as the heat source when energized, thus, the length of the electrode determines the length of the heat source (L_s). Different from the above calculations, the material difference and TBR are taken into consideration to improve the accuracy of the simulation [54]. The thermal conductivity of SiC is set to be 3 times to that of GaN, and TBR is described by the diffuse mismatch model [55]. The boundary conditions are given temperature on the bottom side, adiabatic on the other three sides. To capture phonon ballistic transport and interfacial heat transfer, the top MC zone of the hybrid MC-diffusion method includes the entire GaN layer and a region of two phonon MFP thicknesses in the SiC layer. TBR is treated as the phonon transmission and reflection interface condition [56,57]. Owing to the huge computational cost of simulating the SiC layer whose thickness is close to the millimeter scale, phonon MC simulation is nearly impossible and cannot be used to validate the hybrid method. As an alternative, the simulation results are compared with the experimental results in references.

The temperature distribution of the GaN-on-SiC sample looks like the results shown in Fig. 5, the outline of the high-temperature area is narrow and long under the action of thermal spreading effect and ballistic effect. The main difference is that isotherms become discontinuous at the interface, which is caused by the TBR between GaN and SiC. The temperature discontinuity at the material interface can be observed obviously in the temperature distribution along the vertical symmetry line, making the channel peak temperature higher than the case without TBR. In addition, the temperature gradients in the GaN layer and the SiC layer are different as a result of different thermal conductivity. The comparison between our simulated peak temperature and the reported experimental data [12,58] is shown in Fig. 9, in which the results are transformed into the ratio of the simulated/experimental peak temperature to the ones predicted by FEM. Such a ratio is deemed to directly reflect the effect of phonon ballistic transport [11,41,43,58] as it avoids the possible errors caused by other factors, like different device structures and material

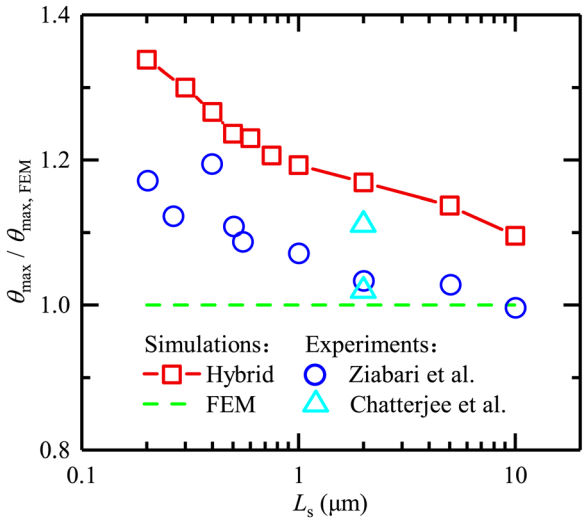

Fig. 9 The ratio of θ_{max} varying with L_s. The experimental data are extracted from Refs. [12] and [58].

Downloaded from http://asmedigitalcollection.asme.org/electronicpackaging/article-pdf/145/1/011203/6976220/ep_145_01_011203.pdf by Tsinghua University user on 01 February 2023

properties. The simulated and measured values of $\theta_{max}/\theta_{max,FEM}$ are all greater than 1, indicating the appearance of phonon ballistic transport. Moreover, $\theta_{max}/\theta_{max,FEM}$ increases with L_s decreasing, which is consistent with the conclusion that a smaller heat source length corresponds to a stronger ballistic effect [43]. The qualitative agreement between the simulations and the experiments verifies the validation of the hybrid MC-diffusion method and the use of the HS scheme to model self-heating. The quantitative deviation is probably due to the differences in phonon properties and heat source sizes. A more rigorous simulation by the hybrid method will be conducted in the future, which is expected to have better consistency with experiments.

3.2 Thermal Spreading Resistance of Different Heating Schemes. With the help of the hybrid method, it is possible to conduct in detail studies about the different ways of modeling self-heating, including the cases with relatively large system thicknesses. To avoid the impact of heating power on junction temperature, the total thermal spreading resistance is introduced, which is calculated using the average temperature rise of the heat generation region [20]:

$$R = \frac{\int_{\text{heating region}} (T - T_0)\mathrm{d}V}{\dot{Q}_s L_s t_s} \tag{1}$$

The current problem involves four factors that may jointly determine the thermal spreading resistance: (1) the thermal spreading effect that is associated with the system shape; (2) the cross-plane ballistic effect that is controlled by the system thickness; (3) the lateral ballistic effect that occurs because the width of the heat generation region is comparable with the phonon MFP; and (4) the ballistic effect that depends on the thickness of the heat generation region. Our previous work [43] investigated the effects of the first three factors in the HF scheme and established a semi-empirical thermal spreading resistance model as $R_{HF} = R_F\left(1 + \frac{2}{3}\mathrm{Kn}_t\right)(1 + A_L \mathrm{Kn}_{L,s})$, which is dependent on L/t, L_s/L, and Kn_t. In the HS scheme, when the thickness of the heat generation region, t_s, is comparable to the phonon MFP, the fourth factor could produce a new kind of ballistic effect and affect the thermal spreading resistance. Since our attention is given to the dependence of phonon transport on $\mathrm{Kn}_{t,s}$, all the calculations in this section are conducted under the same values of $L_s/L = 0.01$ and $L/t = 40$ regardless of the material difference and TBR. As mentioned in Sec. 3.1, for the cases of relatively large system thicknesses ($\mathrm{Kn}_t \le 0.2$), the hybrid MC-diffusion method is utilized; for the cases of relatively small system thicknesses ($\mathrm{Kn}_t > 0.2$), MC simulation is a preferable choice.

The dimensionless thermal spreading resistance, $R^* = R/R_{1D,0}$, varying with the system thickness is shown in Fig. 10(*a*), where the results for $\mathrm{Kn}_t \le 0.2$ are more distinctly demonstrated in Fig. 10(*b*). It is found that the heating scheme indeed plays an important role in the thermal spreading resistance, and the influence is closely related to Kn_t. The dimensionless thermal resistance based on Fourier's law, R^*_{FEM}, is determined by the system shape, which is controlled by L_s/L, L/t and t_s/t, so it will not vary with Kn_t, as the constant lines in Fig. 10 exhibit. When the heating scheme changes, R^*_{FEM} varies with the heat source thickness. For $t_s/t \le 0.01$, the dimensionless thermal resistance in the HS scheme is $R^*_{FEM,HS} \approx 33.5$, which is almost the same as the value of the HF scheme ($R^*_{FEM,HF} = 33.1$). With t_s/t rising, $R^*_{FEM,HS}$ declines. For example, $R^*_{FEM,HS} = 28.7$ at $t_s/t = 0.1$ is about 10% less than $R^*_{FEM,HF}$. The t_s/t-dependent thermal spreading resistance under Fourier's law is attributed to the heat accumulation effect. As t_s/t decreases, heat dissipation is constrained to a thinner region, and more accumulated heat produces a higher junction temperature and larger thermal spreading resistance. When t_s/t is small enough, say $t_s/t \le 0.01$, the heat generation region can be approximately viewed as a "line." As a result, $R^*_{FEM,HS}$ approaches $R^*_{FEM,HF}$.

In ballistic-diffusive regime, ballistic effect amplifies the thermal spreading resistance; thus, the symbols in Fig. 10 lie above the lines. Considering the t_s/t dependence of R^* in Fourier's law, $\mathrm{Kn}_{t,s}$ is not explicitly exhibited because $\mathrm{Kn}_{t,s} = \frac{\mathrm{Kn}_t}{t_s/t}$. For $\mathrm{Kn}_t = 0.01$, the thickness is so large that most phonons are transported diffusively, and R^* of the hybrid MC-diffusion method compares favorably to the FEM solutions. As Kn_t advances, phonon ballistic transport appears and the dimensionless thermal spreading resistances are greater than the results of FEM, but the strength of ballistic effect is associated with t_s/t. The thinner the heat generation region is, the earlier the results of the hybrid MC-diffusion method depart from those of FEM. As presented in Fig. 10(*b*), for $t_s/t = 0.001$, the hybrid method exceeds the FEM solution at $\mathrm{Kn}_t = 0.02$, but for $t_s/t = 0.1$, the departure takes place at $\mathrm{Kn}_t = 0.05$. Furthermore, the difference between the HS scheme and HF scheme also differs as Kn_t alters, especially in the range of $\mathrm{Kn}_t \le 0.2$. For $\mathrm{Kn}_t = 0.01$, R^*_{HS} with $t_s/t \le 0.01$ is

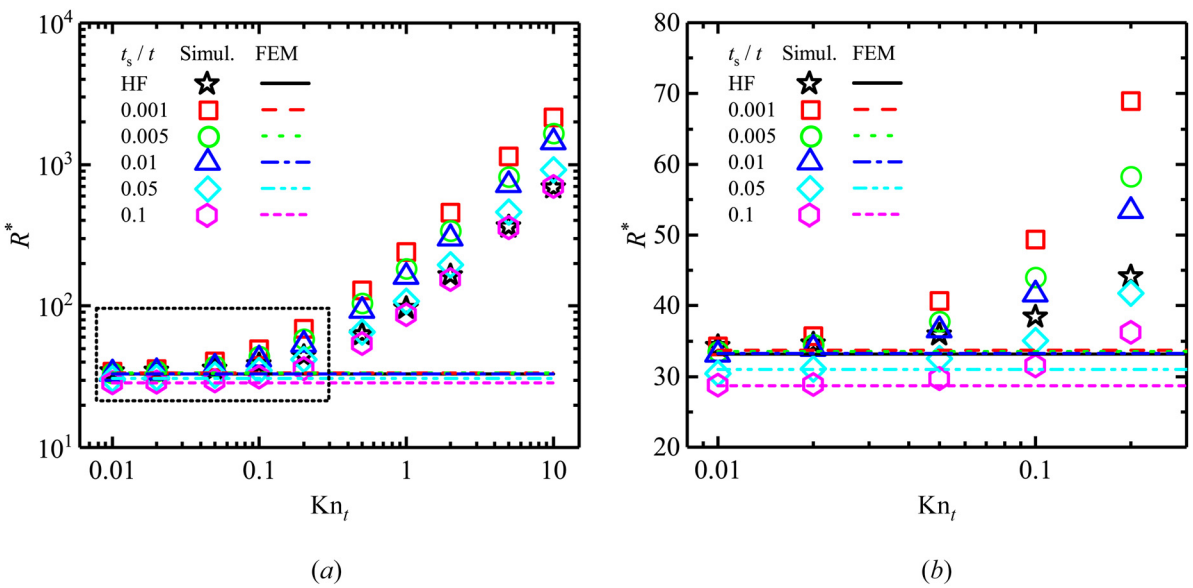

Fig. 10 Dimensionless thermal spreading resistance varying with Kn_t: (*a*) $0.01 \le \mathrm{Kn}_t \le 10$ and (*b*) enlarged at $0.01 \le \mathrm{Kn}_t \le 0.2$. ($L_s/L = 0.01$, $L/t = 40$).

Downloaded from http://asmedigitalcollection.asme.org/electronicpackaging/article-pdf/145/1/011203/6976220/ep_145_01_011203.pdf by Tsinghua University user on 01 February 2023

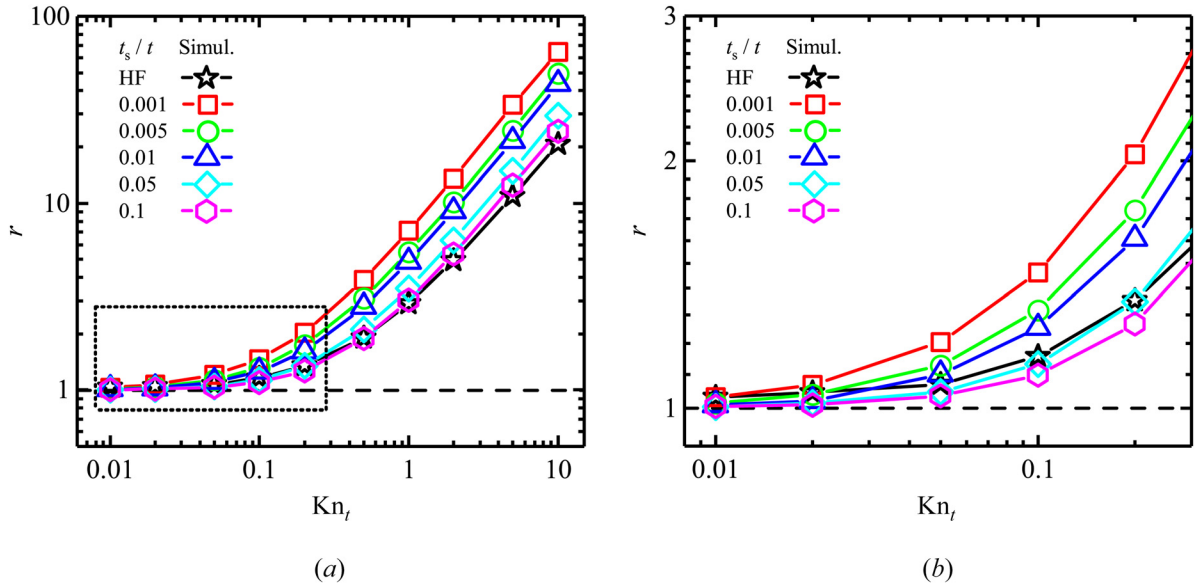

Fig. 11 Thermal spreading resistance ratio varying with Kn_t: (*a*) $0.01 \le Kn_t \le 10$ and (*b*) enlarged at $0.01 \le Kn_t \le 0.2$. ($L_s/L = 0.01$, $L/t = 40$).

almost the same as R^*_{HF}. For $Kn_t = 0.02$, R^*_{HS} with $t_s/t = 0.001$ is slightly larger than R^*_{HF}. When Kn_t increases to 0.05, R^*_{HS} with $t_s/t = 0.005$ also surpasses R^*_{HF}. For $Kn_t = 0.1$, the transcendence of R^*_{HS} with $t_s/t = 0.01$ over R^*_{HF} emerges. For $Kn_t = 0.2$, R^*_{HF} only corresponds to R^*_{HS} with $t_s/t = 0.05$. As Kn_t continues to increase, the profile of R^*_{HF} gets lower. Figure 10(*a*) displays that R^*_{HS} with $t_s/t = 0.1$ is comparable to R^*_{HF} after $Kn_t > 1$. It is illustrative that R^*_{HF} is no longer the upper bound on R^*_{HS} as the ballistic effect strengthens, which is in contrast with what is observed under Fourier's law.

In order to clarify the influence of the heating scheme on phonon ballistic transport, the thermal spreading resistance ratio, $r = R_{Hybrid/MC}/R_{FEM}$, is introduced as we did in Fig. 9, and the results are illustrated in Fig. 11. Here, $R_{Hybrid/MC}$ denotes the thermal spreading resistance calculated by the hybrid method (for $Kn_t \le 0.2$) or MC simulation (for $Kn_t > 0.2$). All the results are larger than 1, and the values move upward as Kn_t increases, indicating the appearance of phonon ballistic transport. It is emphasized that even for relatively large system thicknesses ($Kn_t \le 0.2$), ballistic effect cannot be ignored, as r in Fig. 11(*b*) is definitely greater than 1. Taking the HS scheme with $t_s/t = 0.001$ as an example, $r \approx 1.2$ at $Kn_t = 0.05$ means that using FEM produces an error of 20% in this case. Figure 11 also reveals that the heating scheme adjusts the strength of ballistic effect. In the HS scheme, cutting down t_s/t raises r, and the r profile of the HF scheme gradually becomes lower than the results of the HS scheme with ballistic effect enhancement. For $Kn_t = 0.01$, r_{HF} approximately equals r_{HS} with $t_s/t \le 0.01$. For $Kn_t = 0.05$, r_{HF} is between the values of r_{HS} with $t_s/t = 0.01$ and r_{HS} with $t_s/t = 0.05$. For $Kn_t > 1$, even r_{HS} with $t_s/t = 0.1$ is kind of higher than r_{HF}. Figure 11 proves that reducing the thickness of the heat source yields a stronger ballistic effect, making it possible to overtake the strength of ballistic effect in the HF scheme.

To more directly compare ballistic effect in the HS scheme and the HF scheme, we calculate the ratio of r_{HS} to r_{HF} and get the results displayed in Fig. 12. Starting from 1, the values of r_{HS}/r_{HF} increase with increasing Kn_t, demonstrating again that the HS scheme is able to generate a stronger ballistic effect compared to the HF scheme. A thinner heat generation region will accelerate this process of enlargement. For instance, with $t_s/t = 0.001$, r_{HS}/r_{HF} has been evidently greater than 1 at $Kn_t = 0.1$; however, with $t_s/t = 0.1$, the excess of r_{HS}/r_{HF} on 1 does not turn up until Kn_t is beyond 1. There are even some places where $r_{HS}/r_{HF} < 1$, say, $t_s/t = 0.1$ and $Kn_t = 0.2$.

3.3 Analyses of the Effects of the Heating Scheme. According to the results in Sec. 3.2, it is fair to conclude that the heating scheme does have a powerful impact on the thermal spreading resistance, and the HS scheme with a thinner heat generation region induces stronger phonon ballistic transport than the HF scheme. The findings can be explained as the change in the relative intensity of phonon-boundary scattering at the top boundary. In the HF scheme, heat is generated at the top heat flux boundary, all the motivated phonons move downward, and they have no chance of suffering the scattering of the top boundary unless intrinsic phonon-phonon scattering takes place. However, in the HS scheme, heat is generated inside the system, and the initial phonon movement direction is spatially isotropic. Statistically speaking, half of the phonons go upward after emitting. Since the heat generation region is near the top boundary, almost all upward-moving phonons travel to the top boundary in a ballistic way and suffer phonon-boundary scattering instead of phonon-phonon scattering, which sharply curtails their effective MFPs. As a consequence, the effective thermal conductivity is reduced

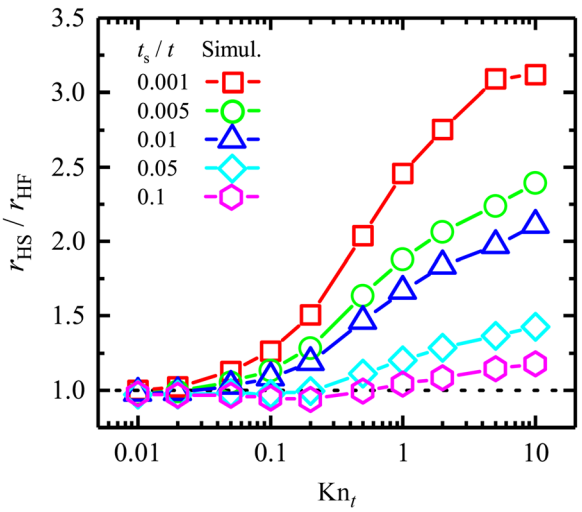

Fig. 12 Ratio of r_{HS} to r_{HF} varying with Kn_t ($L_s/L = 0.01$, $L/t = 40$)

Downloaded from http://asmedigitalcollection.asme.org/electronicpackaging/article-pdf/145/1/011203/6976220/ep_145_01_011203.pdf by Tsinghua University user on 01 February 2023

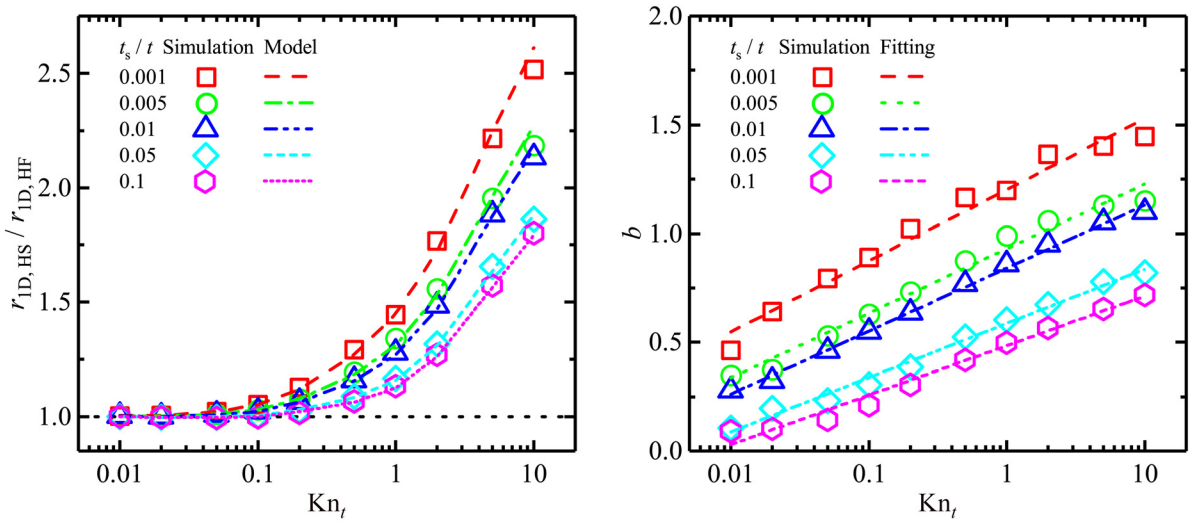

Fig. 13 (*a*) Ratio of r_{HS} to r_{HF} varying with Kn_t in 1D cases and (*b*) the modified values of *b*

[39–41], and the thermal resistance is improved. A greater $Kn_{t,s}$ is supposed to reinforce this kind of heat-source-thickness-related ballistic effect. When the heating scheme changes from HF to HS, on the one hand, the transform of a line heat source to a rectangle heat source diminishes the heat accumulation effect, which is helpful to decrease the thermal spreading resistance; on the other hand, the enhanced scattering at the top boundary provides more boundary confined effects on phonon transport, which raises the thermal spreading resistance. The difference between r_{HS} and r_{HF} is a balance of the two mechanisms. For $Kn_t = 0.01$, phonon-phonon scattering is sufficient to mask the influence of phonon-boundary scattering, and the heat generation region thickness has little effect on the thermal spreading resistance, so $r_{HS}/r_{HF} \approx 1$. As Kn_t increases, the proportion of phonon-boundary scattering increases, and the $Kn_{t,s}$-dependent phonon ballistic transport begins to take effect, resulting in $r_{HS}/r_{HF} > 1$. A small heat generation thickness such as $t_s/t = 0.001$ boosts $Kn_{t,s}$ to be much larger than 1, and $r_{HS}/r_{HF} > 1$ has been visible after $Kn_t \geq 0.05$ in Fig. 12. Raising t_s/t weakens the $Kn_{t,s}$-dependent phonon ballistic transport and delays the point where $r_{HS}/r_{HF} > 1$ happens. In some particular cases where the thermal resistance reduction caused by the thicker heat source covers the enlargement by the strengthened phonon-boundary scattering, r_{HS}/r_{HF} could be less than 1, as the result of $t_s/t = 0.1$ and $Kn_t = 0.2$ in Fig. 12 exhibits.

To test the validity of the analysis, a model about r_{HS}/r_{HF} is established. Disregarding the material difference and TBR has reduced the difficulty of deriving an analytical solution. For the purpose of focusing on the $Kn_{t,s}$-dependent ballistic effect, L_s/L is set to 1 to avoid the interference of the thermal spreading effect and heat-source-width-dependent ballistic effect. Under this condition, the problem degenerates to 1D heat conduction with a small heating region, and phonon BTE can be analytically solved with some approximations. Considering the heat is conducted in the z direction, the 1D form of phonon BTE is written as

$$v_{g,z}\frac{\partial f}{\partial z} = \frac{f_0 - f}{\tau} + \dot{S}_\Omega, \quad 0 \leq z \leq t_s \tag{2a}$$

$$v_{g,z}\frac{\partial f}{\partial z} = \frac{f_0 - f}{\tau}, \quad t_s \leq z \leq t \tag{2b}$$

Here, $v_{g,z} = v_g \cos\theta$ in which θ is the angle between the phonon traveling direction and the z direction, and v_g, f, f_0, τ, and $\dot{S}_\Omega$ denote the phonon group velocity, phonon distribution function, equilibrium distribution function, relaxation time and phonon source per solid angle, respectively. To solve Eq. (2), the distribution function is divided into two parts, $f = f_s + f_d$ [41], in which f_s is the source-induced part that will be solved by the two-flux approximation and f_d is the diffusive part that will be solved by the differential approximation. After a series of mathematical derivations, we have

$$r_{1D,HS} = \frac{R_{1D,HS}}{R_{1D,HS,FEM}} = 1 + \frac{\frac{2}{3} + b}{1 - \frac{2}{3}a}Kn_t = 1 + \alpha \cdot Kn_t \tag{3}$$

in which $a = t_s/t$, $b = \frac{Kn_t}{24a}\left[\exp\left(-2\frac{1+a}{Kn_t}\right) - \exp\left(-2\frac{1-a}{Kn_t}\right) + 2\right] + \frac{Kn_t^2}{48a^2}\left[\exp\left(-4\frac{a}{Kn_t}\right) - 1\right]$. Equation (3) indicates that the thermal resistance ratio can be expressed as a function of the shape factor α and the Knudsen number Kn_t [42]. For the HS scheme, it is reported that $r_{1D,HF} = 1 + \frac{2}{3}Kn_t$ [43]. Thus, we have

$$r_{1D,HS}/r_{1D,HF} = \frac{1 + \alpha Kn_t}{1 + \frac{2}{3}Kn_t} \tag{4}$$

Equation (4) implies that the magnitude relationship between α and $\frac{2}{3}$ decides the value of $r_{1D,HS}/r_{1D,HF}$. Within the range of $t_s/t \in [0.001, 0.1]$, it is always true that $b > 0$ and $\alpha > \frac{2}{3}$. Consequently, the effect of phonon ballistic transport in the HS scheme is more conspicuous than that in the HF scheme.

The results of r_{HS}/r_{HF} in 1D cases calculated by the hybrid MC-diffusion method or MC simulation are depicted in Fig. 13(*a*). The original results of Eq. (4) have some quantitative differences with the simulation results, which is probably proposed by the approximations used in the derivation, like dividing the distribution function, selecting the boundary condition for ballistic-diffusive heat conduction and adopting the differential approximation. To modify the model, we calculate the specific values of b in Eq. (3) by comparing with the simulation, and the obtained results are drawn in Fig. 13(*b*). b is found to increase with Kn_t, and a smaller t_s/t leads to a larger b. Moreover, the linear fitting of $\ln(Kn_t)$ agrees well with the simulation results so that b can be predicted by the fitting functions. Using the fitted values of b, the current model does a reasonably good job of matching the simulation, as the lines in Fig. 13(*a*) shows.

Downloaded from http://asmedigitalcollection.asme.org/electronicpackaging/article-pdf/145/1/011203/6976220/ep_145_01_011203.pdf by Tsinghua University user on 01 February 2023

Although b needs to be modified quantitatively, the expression that $\alpha = \frac{\frac{2}{3}+b}{1-\frac{2}{3}a}$ helps to understand the difference between the HS scheme and the HF scheme. The denominator "$1-\frac{2}{3}a$" reflects the variation of heat source thickness; a greater $a = t_s/t$ means heat is generated in a wider region, the deviation from a "line" heat source is more apparent and α is larger. The numerator "$\frac{2}{3}+b$" reflects the combination of two kinds of phonon ballistic transport, involving the cross-plane ballistic transport represented by "$\frac{2}{3}$" and the heat-source-thickness-dependent ballistic transport represented by "b" (b is explicitly dependent on $\mathrm{Kn}_{t,s} = \mathrm{Kn}_t/a$). The division operation uncovers that there is a tradeoff between the heat accumulation effect and the $\mathrm{Kn}_{t,s}$-related ballistic effect. In the limit case of no thickness heat source ($a = 0$) and no heat-source-thickness-dependent ballistic effect ($b = 0$), Eq. (3) gives $\alpha = \frac{2}{3}$, reproducing the results of the HF scheme. With the benefits of agreeing with electrical simulations and capturing phonon ballistic transport more comprehensively, the HS scheme is concluded to be a better way of modeling self-heating in electronic devices than the HF scheme.

4 Conclusion

In this work, a hybrid phonon MC-diffusion method is applied to simulate self-heating in ballistic-diffusive regime for GaN HEMTs. By setting the MC zones that cover the heat generation region and the boundaries, the hybrid MC-diffusion method captures the elevated junction temperature and the recognizable boundary temperature jump, which are caused by phonon ballistic transport and cannot be observed by Fourier's law. Compared with phonon MC simulation, the hybrid method reduces the computational time up to 2 orders of magnitude at most, while the temperature relative error is less than 5%, which facilitates the fast simulation of ballistic-diffusive heat conduction in relatively large systems ($\mathrm{Kn}_t \leq 0.2$). The performance of the hybrid MC-diffusion method is also verified by the qualitative consistency between the simulations and the reported experiments.

The simulation results suggest that the way of modeling self-heating has a significant impact on phonon transport: the volumetric HS scheme corresponds to a higher junction temperature and thermal spreading resistance than the surface HF scheme as long as Kn_t is large enough, and a thinner heat generation region thickness reinforces this deviation. For $\mathrm{Kn}_t \leq 0.2$, ballistic effect in the HF scheme is roughly equivalent to that in the HS scheme with $t_s/t = 0.05$; for the greater Kn_t, the HS scheme even with $t_s/t = 0.1$ can yield stronger ballistic effect than the HF scheme. The simulation findings are supported by an analytical model based on the 1D phonon BTE.

The dependence of the temperature on the heating scheme is attributed to the relative strength of phonon-boundary scattering in phonon transport. In the diffusive regime, phonon-phonon scattering dominates heat transfer, and the thermal resistance in the HF scheme works as the upper bound of that in the HS scheme since it has the thinnest heat source. However, in the cases where ballistic effect cannot be ignored, phonon boundary scattering at the top boundary in the HS scheme is more intense than in the HS scheme and strengthens with t_s/t, which results in stronger ballistic effect as well as higher junction temperature. The volumetric HS scheme is supposed to reflect the self-heating in GaN HEMTs better, as it agrees with the electrothermal simulations and reproduces the experimentally observed failure of Fourier's law.

Funding Data

- National Natural Science Foundation of China (Nos. U20A20301, 51825601, and 52011530030; Funder ID: 10.13039/501100001809).
- Russian Foundation for Basic Research (No. 20-58-53017; Funder ID: 10.13039/501100002261).

References

[1] Mishra, U. K., Parikh, P., and Wu, Y., 2002, "AlGaN/GaN HEMTs - An Overview of Device Operation and Applications," Proc. IEEE, **90**, pp. 1022–1031.
[2] Hirama, K., Kasu, M., and Taniyasu, Y., 2012, "RF High-Power Operation of AlGaN/GaN HEMTs Epitaxially Grown on Diamond," IEEE Electron Device Lett., **33**(4), pp. 513–515.
[3] Bar-Cohen, A., Albrecht, J., and Maurer, J., 2011, "Near-Junction Thermal Management for Wide Bandgap Devices," IEEE Compound Semiconductor Integrated Circuit Symposium, Waikoloa, HI, Oct. 16–19, pp. 1–5.
[4] Zanoni, E., Meneghesso, G., Verzellesi, G., Danesin, F., Meneghini, M., Rampazzo, F., Tazzoli, A., and Zanon, F., 2007, "A Review of Failure Modes and Mechanisms of GaN-Based HEMTs," IEEE International Electron Devices Meeting, Washington, DC, Dec. 10–12, pp. 381–384.
[5] Meneghesso, G., Verzellesi, G., Danesin, F., Rampazzo, F., Zanon, F., Tazzoli, A., Meneghini, M., and Zanoni, E., 2008, "Reliability of GaN High-Electron-Mobility Transistors: State of the Art and Perspectives," IEEE Trans. Device Mater. Reliab., **8**(2), pp. 332–343.
[6] Stocco, A., 2012, "Reliability and Failure Mechanisms of GaN HEMT Devices Suitable for High-Frequency and High-Power Applications," Ph.D. thesis, University of Padua, Veneto Region, Italy.
[7] Bagnall, K. R., 2013, "Device-Level Thermal Analysis of GaN-Based Electronics," Master's thesis, Massachusetts Institute of Technology, Cambridge, MA.
[8] Paine, B., Polmanter, S., Ng, V., Kubota, N., and Ignacio, C., 2015, "Lifetesting GaN HEMTs With Multiple Degradation Mechanisms," IEEE Trans. Device Mater. Reliab., **15**(4), pp. 486–494.
[9] Sridharan, S., Venkatachalam, A., and Yoder, P. D., 2008, "Electrothermal Analysis of AlGaN/GaN High Electron Mobility Transistors," J. Comput. Electron., **7**(3), pp. 236–239.
[10] Donmezer, N., and Graham, S., 2014, "The Impact of Noncontinuum Thermal Transport on the Temperature of AlGaN/GaN HFETs," IEEE Trans. Electron Devices, **61**(6), pp. 2041–2048.
[11] Donmezer, N., Islam, M., Yoder, D., and Graham, S., 2015, "The Impact of Nongray Thermal Transport on the Temperature of AlGaN/GaN HFETs," IEEE Trans. Electron Devices, **62**(8), pp. 2437–2444.
[12] Chatterjee, B., Dundar, C., Beechem, T. E., Heller, E., Kendig, D., Kim, H., Donmezer, N., and Choi, S., 2020, "Nanoscale Electro-Thermal Interactions in AlGaN/GaN High Electron Mobility Transistors," J. Appl. Phys., **127**(4), p. 044502.
[13] Kennedy, D. P., 1960, "Spreading Resistance in Cylindrical Semiconductor Devices," J. Appl. Phys., **31**(8), pp. 1490–1497.
[14] Won, Y., Cho, J., Agonafer, D., Asheghi, M., and Goodson, K., 2013, "Cooling Limits for GaN HEMT Technology," IEEE Compound Semiconductor Integrated Circuit Symposium, Monterey, CA, Oct. 13–16, pp. 1–5.
[15] Moore, A. L., and Shi, L., 2014, "Emerging Challenges and Materials for Thermal Management of Electronics," Mater. Today, **17**(4), pp. 163–174.
[16] Won, Y., Cho, J., Agonafer, D., Asheghi, M., and Goodson, K., 2015, "Fundamental Cooling Limits for High Power Density Gallium Nitride Electronics," IEEE Trans. Compon., Packag. Manuf. Technol., **5**, pp. 737–744.
[17] Garimella, S. V., Persoons, T., Weibel, J. A., and Gektin, V., 2017, "Electronics Thermal Management in Information and Communications Technologies: Challenges and Future Directions," IEEE Trans. Compon. Packag. Manuf. Technol., **7**(8), pp. 1191–1205.
[18] Fourier, J., 2009, *The Analytical Theory of Heat*, Cambridge University Press, Cambridge, UK.
[19] Krane, M. J. M., 1991, "Constriction Resistance in Rectangular Bodies," ASME J. Electron Packag., **113**(4), pp. 392–396.
[20] Muzychka, Y. S., Culham, J. R., and Yovanovich, M. M., 2003, "Thermal Spreading Resistance of Eccentric Heat Sources on Rectangular Flux Channels," ASME J. Electron Packag., **125**(2), pp. 178–185.
[21] Darwish, A. M., Bayba, A. J., and Hung, H. A., 2004, "Thermal Resistance Calculation of AlGaN-GaN Devices," IEEE Trans. Microwave Theory Tech., **52**(11), pp. 2611–2620.
[22] Muzychka, Y. S., Bagnall, K. R., and Wang, E. N., 2013, "Thermal Spreading Resistance and Heat Source Temperature in Compound Orthotropic Systems With Interfacial Resistance," IEEE Trans. Compon. Packag. Manuf. Technol., **3**(11), pp. 1826–1841.
[23] Gholami, A., and Bahrami, M., 2014, "Thermal Spreading Resistance Inside Anisotropic Plates With Arbitrarily Located Hotspots," J. Thermophys. Heat Transfer, **28**(4), pp. 679–686.
[24] Bagnall, K. R., Muzychka, Y. S., and Wang, E. N., 2014, "Analytical Solution for Temperature Rise in Complex Multilayer Structures With Discrete Heat Sources," IEEE Trans. Compon. Packag. Manuf. Technol., **4**(5), pp. 817–830.
[25] Darwish, A., Bayba, A. J., and Hung, H. A., 2015, "Channel Temperature Analysis of GaN HEMTs With Nonlinear Thermal Conductivity," IEEE Trans. Electron Devices, **62**(3), pp. 840–846.
[26] Pearson, R., Chatterjee, B., Kim, S., Graham, S., Rattner, A., and Choi, S., 2020, "Guidelines for Reduced-Order Thermal Modeling of Multifinger GaN HEMTs," ASME J. Electron. Packag., **142**(2) p. 021012.
[27] Pop, E., Sinha, S., and Goodson, K. E., 2006, "Heat Generation and Transport in Nanometer-Scale Transistors," Proc. IEEE, **94**(8), pp. 1587–1601.
[28] Cahill, D. G., Braun, P. V., Chen, G., Clarke, D. R., Fan, S., Goodson, K. E., Keblinski, P., King, W. P., Mahan, G. D., Majumdar, A., Maris, H. J., Phillpot, S. R., Pop, E., and Shi, L., 2014, "Nanoscale Thermal Transport. II. 2003–2012," Appl. Phys. Rev., **1**(1), p. 011305.
[29] Warzoha, R. J., Wilson, A. A., Donovan, B. F., Donmezer, N., Giri, A., Hopkins, P. E., Choi, S., Pahinkar, D., Shi, J., Graham, S., Tian, Z., and Ruppalt, L.,

Downloaded from http://asmedigitalcollection.asme.org/electronicpackaging/article-pdf/145/1/011203/6976220/ep_145_01_011203.pdf by Tsinghua University user on 01 February 2023

2021, "Applications and Impacts of Nanoscale Thermal Transport in Electronics Packaging," ASME J. Electron. Packag., **143**(2), p. 020804.
[30] Ma, J. L., Wang, X. J., Huang, B. L., and Luo, X. B., 2013, "Effects of Point Defects and Dislocations on Spectral Phonon Transport Properties of Wurtzite GaN," J. Appl. Phys., **114**(7), p. 074311.
[31] Freedman, J. P., Leach, J. H., Preble, E. A., Sitar, Z., Davis, R. F., and Malen, J. A., 2013, "Universal Phonon Mean Free Path Spectra in Crystalline Semiconductors at High Temperature," Sci. Rep., **3**(1), p. 2963.
[32] Ziade, E., Yang, J., Brummer, G., Nothern, D., Moustakas, T., and Schmidt, A. J., 2017, "Thickness Dependent Thermal Conductivity of Gallium Nitride," Appl. Phys. Lett., **110**(3), p. 031903.
[33] Chen, G., 1998, "Thermal Conductivity and Ballistic-Phonon Transport in the Cross-Plane Direction of Superlattices," Phys. Rev. B, **57**(23), pp. 14958–14973.
[34] Maznev, A. A., Cuffe, J., Eliason, J. K., Minnich, A. J., Kehoe, T., Torres, C. M. S., Chen, G., Nelson, K. A., and Johnson, J. A., 2013, "Direct Measurement of Room-Temperature Nondiffusive Thermal Transport Over Micron Distances in a Silicon Membrane," Phys. Rev. Lett., **110**(2), p. 025901.
[35] Chen, G., 1996, "Nonlocal and Nonequilibrium Heat Conduction in the Vicinity of Nanoparticles," ASME J. Heat Transfer-Trans. ASME, **118**(3), pp. 539–545.
[36] Schleeh, J., Mateos, J., Íñiguez-de-la Torre, I., Wadefalk, N., Nilsson, P. A., Grahn, J., and Minnich, A. J., 2015, "Phonon Black-Body Radiation Limit for Heat Dissipation in Electronics," Nat. Mater., **14**(2), pp. 187–192.
[37] Hua, Y. C., and Cao, B. Y., 2014, "Phonon Ballistic-Diffusive Heat Conduction in Silicon Nanofilms by Monte Carlo Simulations," Int. J. Heat Mass Transfer, **78**, pp. 755–759.
[38] Li, H. L., and Cao, B. Y., 2019, "Radial Ballistic-Diffusive Heat Conduction in Nanoscale," Nanoscale Microscale Thermophys. Eng., **23**(1), pp. 10–24.
[39] Cao, B. Y., and Li, Y. W., 2010, "A Uniform Source-and-Sink Scheme for Calculating Thermal Conductivity by Nonequilibrium Molecular Dynamics," J. Chem. Phys., **133**(2), p. 024106.
[40] Li, Y. W., and Cao, B. Y., 2013, "Thermal Conductivity of Single-Walled Carbon Nanotube With Internal Heat Source Studied by Molecular Dynamics Simulation," Int. J. Thermophys., **34**(12), pp. 2361–2370.
[41] Hua, Y. C., and Cao, B. Y., 2016, "The Effective Thermal Conductivity of Ballistic-Diffusive Heat Conduction in Nanostructures With Internal Heat Source," Int. J. Heat Mass Transfer, **92**, pp. 995–1003.
[42] Hua, Y. C., and Cao, B. Y., 2016, "Ballistic-Diffusive Heat Conduction in Multiply-Constrained Nanostructures," Int. J. Therm. Sci., **101**, pp. 126–132.
[43] Hua, Y. C., Li, H. L., and Cao, B. Y., 2019, "Thermal Spreading Resistance in Ballistic-Diffusive Regime for GaN HEMTs," IEEE Trans. Electron Devices, **66**(8), pp. 3296–3301.
[44] Bao, H., Chen, J., Gu, X. K., and Cao, B. Y., 2018, "A Review of Simulation Methods in Micro/Nanoscale Heat Conduction," ES Energy Environ., **1**, pp. 16–55.
[45] Choi, S., Graham, S., Chowdhury, S., Heller, E. R., Tadjer, M. J., Moreno, G., and Narumanchi, S., 2021, "A Perspective on the Electro-Thermal co-Design of Ultra-Wide Bandgap Lateral Devices," Appl. Phys. Lett., **119**(17), p. 170501.
[46] Hao, Q., Zhao, H., and Xiao, Y., 2017, "A Hybrid Simulation Technique for Electrothermal Studies of Two-Dimensional GaN-on-SiC High Electron Mobility Transistors," J. Appl. Phys., **121**(20), p. 204501.
[47] Hao, Q., Zhao, H. B., Xiao, Y., Wang, Q., and Wang, X. L., 2018, "Hybrid Electrothermal Simulation of a 3-D Fin-Shaped Field-Effect Transistor Based on GaN Nanowires," IEEE Trans. Electron Devices, **65**(3), pp. 921–927.
[48] Hao, Q., Zhao, H., Xiao, Y., and Kronenfeld, M. B., 2018, "Electrothermal Studies of GaN-Based High Electron Mobility Transistors With Improved Thermal Designs," Int. J. Heat Mass Transfer, **116**, pp. 496–506.
[49] Li, H. L., Hua, Y. C., and Cao, B. Y., 2018, "A Hybrid Phonon Monte Carlo-Diffusion Method for Ballistic-Diffusive Heat Conduction in Nano- and Micro-Structures," Int. J. Heat Mass Transfer, **127**, pp. 1014–1022.
[50] Li, H. L., Shiomi, J., and Cao, B. Y., 2020, "Ballistic-Diffusive Heat Conduction in Thin Films by Phonon Monte Carlo Method: Gray Medium Approximation Versus Phonon Dispersion," ASME J. Heat Transfer-Trans. ASME, **142**(11), p. 112502.
[51] Shen, Y., Hua, Y. C., Li, H. L., Sobolev, S. L., and Cao, B. Y., 2022, "Spectral Thermal Spreading Resistance of Wide Bandgap Semiconductors in Ballistic-Diffusive Regime," IEEE Transactions on Electron Devices, **69**(6), pp. 3047–3054.
[52] Hua, Y. C., and Cao, B. Y., 2017, "Slip Boundary Conditions in Ballistic-Diffusive Heat Transport in Nanostructures," Nanoscale Microscale Thermophys. Eng., **21**(3), pp. 159–176.
[53] Peraud, J. P. M., and Hadjiconstantinou, N. G., 2011, "Efficient Simulation of Multidimensional Phonon Transport Using Energy-Based Variance-Reduced Monte Carlo Formulations," Phys. Rev. B, **84**(20), pp. 1555–1569.
[54] García, S., Íñiguez-de-la-Torre, I., Mateos, J., González, T., and Pérez, S., 2016, "Impact of Substrate and Thermal Boundary resistance on the Performance of AlGaN/GaN HEMTs Analyzed by Means of Electro-Thermal Monte Carlo Simulations," Semicond. Sci. Technol., **31**(6), p. 065005.
[55] Pohl, R. O., and Swartz, E. T., 1989, "Thermal Boundary Resistance," Rev. Mod. Phys., **61**(3), pp. 605–668.
[56] Hua, Y. C., and Cao, B. Y., 2018, "Interface-Based Two-Way Tuning of the in-Plane Thermal Transport in Nanofilms," J. Appl. Phys., **123**(11), p. 114304.
[57] Ran, X., Guo, Y., and Wang, M., 2018, "Interfacial Phonon Transport With Frequency-Dependent Transmissivity by Monte Carlo Simulation," Int. J. Heat Mass Transfer, **123**, pp. 616–628.
[58] Ziabari, A., Torres, P., Vermeersch, B., Xuan, Y., Cartoixà, X., Torelló, A., Bahk, J.-H., Koh, Y. R., Parsa, M., Ye, P. D., Alvarez, F. X., and Shakouri, A., 2018, "Full-Field Thermal Imaging of Quasiballistic Crosstalk Reduction in Nanoscale Devices," Nat. Commun., **9**(1), p. 255.

Downloaded from http://asmedigitalcollection.asme.org/electronicpackaging/article-pdf/145/1/011203/6976220/ep_145_01_011203.pdf by Tsinghua University user on 01 February 2023